Steam batch thermal processes in unsteady state conditions: Modelling and application to a case study in the food industry

A. Biglia, L. Comba, E. Fabrizio, P. Gay, D. Ricauda Aimonino

Volume 118, Elsevier, 2017, pag. 638 - 651

Steam batch thermal processes in unsteady state conditions: Modelling and application to a case study in the food industry

Abstract

Many industrial processes require high amounts of steam. Design and operation of steam plants are particularly complex when the steam supply is required for short periods and with a varying time schedules. To fulfil the discontinuous needs of steam users, avoiding the steam boiler oversizing to the peak value of the steam request, a thermal energy storage (TES) system can be adopted. The proper sizing of TES systems, which, in this application, is constituted by a steam accumulator vessel installed between the steam generator and the consumer, cannot be based on the sole initial and final state conditions of the steam storage, since a performance prediction of the process time-evolution is also required.
In this paper, a model of steam batch processes for industrial thermal treatments, able to describe unsteady operative conditions, is presented. More in detail, a three-stage steam plant, with a sequentially interconnected steam boiler, steam accumulator and processing tank, has been considered. The dynamic model of the charging and discharging processes of the steam accumulator has been applied to a real case study in the food industry: the batch debacterisation process of cocoa beans. Nevertheless, the obtained results can be profitably employed in the design and the performance assessments of a wide set of applications involving the steam processing fluid, such as desalination plants, solar thermal power plants, retorts, steam ovens and others.

Keywords: Steam batch process; Steam accumulator; Tank steam filling; Unsteady process; Food industry

1. Introduction

The adoption of steam as a heat carrier is affirmed in many industrial thermal processes [1-3], thanks to the high value of latent energy per unit of mass [4] which, during the condensation, is available to be transferred at a constant temperature and with a very high heat transfer coefficient. When the thermal energy required by the consumers is low compared with production, the produced steam can be accumulated in insulated tanks, implementing a thermal energy storage (TES) system [5]. Therefore, steam is a convenient energy carrier, even if its production is rather expensive. To ensure the steam boiler optimal working condition is thus essential in order to increase the system efficiency, which results in a consequent less expensive steam production [6]. This can be achieved by coupling the steam boiler with a TES system, which increases the energy efficiency by managing the demand-side. Several profitable applications of TES systems can be found in literature [7-12], where TES system are adopted to lower, smooth or shift the thermal, electrical or cooling load time profile.
In industrial applications, steam can be saturated or superheated. Usually, superheated steam is adopted to prevent condensation during its distribution, due to a decrease in temperature under the saturation value, at the particular processing pressure [13-14]. Thanks to its capability to quickly heat up the food product surface, due to the high quantity of thermal energy transmitted per unit of time, steam is widely employed in thermal food industrial processes. Indeed, with the involved high temperatures, undesired pre-cooking process may occur in the presence of a too slow heat exchange between food products and the carrier fluid. Moreover, with respect to hot air systems, the adoption of steam can reduce oxidation phenomena [15], even if the possible condensation phenomena on the product surfaces, when undesired, is a not negligible disadvantage.

In many cases, the amount of steam required at the use-side, in terms of instantaneous flow rate, is not constant. Batch processes, as e.g. retort sterilisation or debacterisation, require a huge amount of steam for short periods of time. Since steam boilers cannot react instantaneously to demand variations, usually they are sized on the base of the peak demand value, resulting in an oversized design. A TES system, based on the flash steam accumulator technology, could be adopted in order to: (1) fulfil the peak demands that occur for short time periods; (2) protect the steam boiler from operating under capacity [16].
An application where the coupling between a steam boiler and a steam accumulator represents an effective solution is the one of solar thermal power plants [17-20]. During periods of low solar radiation, the heat stored in the steam accumulator is discharged, while, during periods of high solar radiation, the excess part of the produced steam is used to recharge the steam accumulator.
For these reasons, the adoption of steam accumulators results to be essential in those processes where the supply of huge amount of steam is required for limited periods of time, with respect to an average working cycle values, and/or where the energy source is intermittent.
In the food industry, many effective applications of the coupling between a steam boiler and a steam accumulator can be found. Several industrial food processes require the supplying of large quantities of saturated or superheated steam during short periods of time, maybe with a particular time schedule. This is the case, for example, of batch pasteurisation and sterilisation processes for retort, debacterisation, blanching, etc. With different temperatures and time durations, all these examples are representative of thermal processes applied to food products with the goal of reducing microbial charge and enzymatic activity to stabilize the product and reducing quality deterioration.
In this paper, a model of steam batch processes for industrial thermal treatments, able to describe unsteady operative conditions, is presented. More in detail, a three-stage steam plant, with a sequentially interconnected steam boiler, steam accumulator and processing tank, has been considered. The objective of the model is to predict the working condition of the various components of the systems (steam accumulator, connection pipe and processing tank) with different sizing and initial conditions, the pressurisation of the processing tank and the heat exchange between the vapour and the product to be processed. The time evolution of the steam temperature and pressure in the accumulator, the steam accumulator volume, the steam boiler capacity, the volume and the time evolution of temperature and pressure of the processing tank are some of the features provided by the application of the proposed model.
The proposed model demonstrates its effectiveness as a design tool, employable during plant sizing or to verify the operating conditions and the energy requirements of a given plant. Indeed, the model allows to study the proper trade-off between the steam boiler capacity, the steam accumulator volume and the processing tank volume and others design parameter, predicting the performance on the entire process.
The assumptions and simplifications adopted in the modelling framework, discussed in section § 3, are related to the required level of detail. Regarding the steam accumulator, for instance, different modelling approaches exist. A simple one, based to the sole initial and final conditions of the accumulator, in terms of pressure or temperature [17], provides result only suitable for a preliminary rough sizing of the component.
In order to evaluate the dynamic evolution of the temperature and pressure in the steam accumulator, models based on the equilibrium and non-equilibrium conditions between the vapour and liquid phases were developed. In the equilibrium model [20], the vapour and liquid phases are considered at the same saturation temperature and pressure, allowing to determine the complete thermodynamic state of the steam accumulator as a function of the sole pressure or temperature. Moreover, during thermodynamic change the evaporation and condensation rates are considered instantaneous. Lately, studies aiming at

defining the dynamic behaviour of the steam accumulator, considering the nonlinear non-monotonic changing phenomenon that modifies the equilibrium solution, have been conducted [21-23]. This latter approach requires to separately consider the pressure and temperature evolutions of the two water phases (liquid and vapour) in the accumulator and to compute the evaporation and condensation finite rates defining two parameters, the evaporation and condensation relaxation times, which were obtained through empirical procedures. Indeed, as described in [22], different initial conditions of the steam accumulator (e.g. in terms of water filling ratio, of pressure, of temperature etc.) leads to a not predictable variation in the value of these two parameters. Considering that the scope of this article is to predict the behaviour – for design purposes – of a complex system where the steam accumulator is one component, and since the two evaporation and condensation relaxation times are experimental parameters which are unknown and cannot be precisely estimated before implementing a steam accumulator, in our work a dynamic model based on equilibrium conditions between the two phases was adopted for the steam accumulator.
The developed modelling framework has been applied to a real case study of the food industry: a cocoa beans debacterisation plant. The considered steam plant is composed by a steam boiler, a steam accumulator and a debacterisation tank.
The paper is organized as follows: the technological features and the operating principles of the steam loop system are presented in Section 2; Section 3 introduces the balance equations integrated in the model while, in Section 4, the model is applied to a case study. Finally, the conclusions are reported in the last section.

2. Description of the technology

In order to describe the developed model, an illustrative three-stage steam plant is introduced, which is constituted by a sequentially interconnected steam boiler, steam accumulator and processing tank (Fig. 1). The steam flow rates $\dot{m}_{12,v}$, from the steam boiler to the steam accumulator, and $\dot{m}_{23,v}$, from this last to the processing tank, are regulated by valves ψ_1 and ψ_2 respectively.
The steam produced by the boiler is injected through a set of nozzles into the lower edge of the steam accumulator. During the charging phase of the accumulator, the incoming steam, injected under the surface level of the water already presents in the accumulator, rapidly condensates leading to an increment of the pressure p_2 and temperature T_2 of the accumulator. The charging process occurs at the initial start-up, when the water contained in the accumulator is in equilibrium with the environment temperature, or when the temperature and/or the pressure values in the accumulator decrease below certain thresholds. Once the steam accumulator is pressurised, the downstream valve ψ_2 is opened when a supply of steam is required. The steam flow rate from the accumulator to the processing tank, which is affected by the pressure difference between the two interconnected tanks, p_2 and p_3 respectively, can be intercepted by closing the valve ψ_2 when the thermal process does not require additional heat. The processing tank contains the food product, properly arranged to be treated by the steam.

2.1 Steam accumulator

A steam accumulator is made by a pressurised vessel and it is generally used as buffer storage when the load demand of steam is discontinuous, e.g. with temporary high flow rate for short periods of time, also with fast dynamics. In this way, the sizing of the steam boiler can be limited to the average steam load value, with respect to a standard working cycle, avoiding an oversizing to cover the peak value. With this

solution, the steam boiler will charge the accumulator with continuity, ever working at its optimal efficiency.

However, since the density $\rho_{2,v}$ of saturated steam is significantly lower than saturated liquid one $\rho_{2,l}$, directly storing saturated or superheated steam (dry accumulator) requires higher storing volumes with respect to vessel containing saturated liquid water (wet accumulator). In the case of wet accumulator, the steam is produced by a pressure reduction in a pressurised storage of saturated liquid and vapour water, resulting in a not constant pressure steam production (sliding pressure steam accumulators). The process of fast evaporation caused by lowering the pressure is called flashing, which produces flash steam. In steam plants, flash tanks are also adopted for heat recovery of the steam condensate drainage; in this case, vertical flash tanks are preferred since the enhanced separation provided between steam and water [24-25]. It should be noted that the flash steam production rate is limited by an upper boundary limit depending on the surface area of the liquid-vapour interface. Reference curves that express the maximum flash steam generation velocity per square meter of interface surface as a function of the pressure can be found in technical literature. For this reason, in order to increase the flash steam production rate for a given water mass, horizontal vessels are usually preferred to vertical ones, because of the more favourable liquid-vapour interface surface.

The sliding pressure steam accumulator (Fig. 1) contains steam and liquid water which are heated by the steam boiler during the charging process. When the discharging process starts, the out coming steam flow rate $\dot{m}_{23,v}$ leads to a pressure reduction in the accumulator and, consequently, to the evaporation of a portion of liquid in order to re-equilibrate the system. The high specific heat capacity and the low specific volume of liquid water allow great quantities of heat to be stored in the vessel and, therefore, a large quantity of steam to be produced.

The amount of produced steam depends on the initial and final pressure values of the discharge process. Usually, the lower $p_{2,min}$ and maximum $p_{2,max}$ pressure values of steam accumulator should not decrease or exceed the values specified by the required thermal process. The value of the two pressure limits $p_{2,min}$ and $p_{2,max}$ can give a first rough design of a steam accumulator can be done by defining the producible amount of flash steam $m_{2,v}$ as

$$m_{2,v} = \frac{m_{2,l} \cdot (h_{2,max} - h_{2,min})}{\Lambda} \quad (1)$$

where $m_{2,l}$ represents the liquid water mass in the steam accumulator before the steam production, $h_{2,min}$ and $h_{2,max}$ the enthalpy of $m_{2,l}$ at pressure $p_{2,min}$ and $p_{2,max}$ respectively, and Λ the latent heat of water. Eq. (1), however, does not take into account the evolution of the accumulator pressure and temperature over time, during both charging and discharging processes.

2.2 Processing tank

Several non-stationary food processes can be schematized by the considered illustrative plant (Fig. 1): in the final steam user, the processing tank downstream the steam accumulator, a microbial decontamination, a bleaching or a cooking process, such as a steam oven cooking, can take place. Nowadays, the steam oven cooking is one of the widely-adopted cooking process in food industry, particularly widespread in commercial processing and food service operation, thanks to the provided good quality of the cooked products by the steam contact [26]. The effectiveness of steam ovens has been proved by numerous studies: Bowers et al. [27] investigated the positive effects of moist-heat with respect to the dry-heat cookery while Mora et al. [28] compared the cooking results in the case of ovens with forced convection, with low steam or with high steam, at a temperature of 100 °C, noting good effects in

terms of reduction of cooking time and reduction of dehydration phenomena, which usually occur with traditional oven cooking. The considered processing tank can also represent another food industry batch process: the steaming [29]. This type of cooking, affirmed as one of the healthiest cooking techniques, is widely used e.g. in the preparation of Asian cuisines.
In the food industry, steam is also used to pressurise retorts in order to perform steam sterilisation cycles [30-32]. Lau et al. in [30] have developed and validated a numerical model of a retort, which allows to predict the transient vessel temperature and pressure profiles of an entire steam sterilisation cycle. Singh et al. [31] conducted a set of experiments for evaluating the heat transfer phenomena inside a conventional static steam retort. An evaluation of the energy consumption in a steam retort has been performed by Berteli et al. [32], comparing the conventional and alternative venting processes.

3. Modelling framework

3.1 Steam boiler model

In this study, the steam boiler has been considered as an ideal steam generator, producing a stationary steam flow rate $\dot{m}_{12,v}$, at constant pressure p_1 and temperature T_1, when it is active. The produced steam flow, characterized by a certain enthalpy $h_{1,v}$, reaches the downstream steam accumulator through the valve ψ_1, which is kept open until the pressure p_2 of the steam accumulator does not exceed the maximum allowed value $p_{2,max}$.

3.2 Steam accumulator model

A steam wet accumulator can be modelled as a pressurised vessel containing liquid and vapour water. Considering the dynamic of the water evaporation and of the steam condensation much faster than the charging and discharging processes, the water-vapour accumulator system is considered in thermodynamic equilibrium and, thus, the accumulator thermodynamic state can be completely defined by its temperature or pressure. The mass of liquid water $m_{2,l}$ in the accumulator is function of the volumetric filling fraction of water $\xi_{2,l}$, of the steam accumulator volume V_2 and of the water density $\rho_{2,l}$.
The state of the steam accumulator has been described by the following two state variables: the mass m_2, which is the sum of the water mass and vapour mass content, and the overall internal energy U_2, in accordance with literature works [33].
Considering that charging and discharging processes of the steam accumulator may simultaneously occur, the accumulator mass balance is

$$\frac{dm_2}{dt} = \dot{m}_{12,v} - \dot{m}_{23,v} \quad (2)$$

where $\dot{m}_{12,v}$ is the accumulator inlet steam flow rate and $\dot{m}_{23,v}$ the steam flow rate provided to the consumer, described in § 3.4.
The energy balance in the steam accumulator control volume, neglecting the kinetic and potential energy effects, is

$$\frac{dU_2}{dt} = \dot{Q}_{2,e} + \dot{m}_{12,v}h_{1,v} - \dot{m}_{23,v}h_{2,v} \quad (3)$$

where $\dot{m}_{12,v}h_{1,v}$ and $\dot{m}_{23,v}h_{2,v}$ represent the energy flow rate entering and exiting the steam accumulator, respectively. The heat transfer $\dot{Q}_{2,e}$ rate, introduced to account for the vessel thermal losses, is a function of the external surface A_2 and the thermal transmittance K_2 of the accumulator, as

$$\dot{Q}_{2,e} = A_2K_2(T_e - T_2) \quad (4)$$

where T_e is the environment temperature, which has been considered constant.

The dynamic of the accumulator is therefore described by the two differential equations Eq. (2) and Eq. (3). Considering the internal dynamics of the steam accumulator as a succession of equilibrium conditions between the vapour and the liquid phases, the pressure p_2 and vapour quality x_2 can be determined by assuring the saturation condition, solving the system of non-linear equations

$$\begin{cases} V_2 = m_2 \left(x_2 \cdot v_{2,v}(p_2) + (1 - x_2) \cdot v_{2,l}(p_2) \right) \\ U_2 = m_2 \left(x_2 \cdot u_{2,v}(p_2) + (1 - x_2) \cdot u_{2,l}(p_2) \right) \end{cases} \quad (5)$$

The specific volume v and specific internal energy u, of both liquid and vapour phases were computed by a set of splines interpolating functions, using the Wagner & Kretzschmar [34] steam data table as nodes. Finally, the others thermodynamic properties of the steam accumulator can be easily evaluated as a function of the sole pressure.

3.3 Processing tank model

During the filling phase of the processing tank by means of the steam flow rate $\dot{m}_{23,v}$, the steam pressure p_3 and temperature $T_{3,v}$ evolutions are linked. Indeed, the incoming high pressure steam flow performs a compression work to the low pressure air/steam mixture, leading to an increase of the internal energy $U_{3,v}$, and consequently of $T_{3,v}$ [35]. Moreover, during the food processing, a portion of the steam internal energy is being transferred to the food product, through a thin film of water, resulting from a condensation phenomenon on the food surfaces.
The developed thermodynamic model of the processing tank, during the filling process, takes into account two concurrent aspects: (1) the steam temperature and pressure evolution inside the tank during the pressurisation process and (2) the heat exchange from the vapour to the food product.

3.3.1 Steam state evolution

The dynamic of the steam into the processing tank is described by the variables $T_{3,v}$ and p_3.
Several thermodynamic analyses of the filling phase of tanks can be found in literature, in particular for the cases of hydrogen and natural gas. In the work of Ruffio et al. [36], temperature and pressure evolutions during tank filling have been derived from thermodynamic database (NIST) and by three different equations of state (EoS). Results obtained with Redlich-Kwong EoS and with NIST database were in good agreement. The refilling process of a gaseous hydrogen tank was modelled in [37] and [38], where a compressibility factor has been defined to take into account the real behaviour of the gas. Moreover, regarding the fast filling process of hydrogen storage cylinders, in [39] and [40], experimental trials have been carried out to investigate the concurrent increased of temperature and pressure as a function of different parameters.
In the present work, temperature and pressure dynamics are studied by combining the Redlich-Kwong EoS with the first law of thermodynamics. Using the first law of thermodynamics for an open system the derivative of the internal energy $U_{3,v}$, expressed as the product of mass $m_{3,v}$ and specific internal energy $u_{3,v}$, is

$$\frac{dU_{3,v}}{dt} = m_{3,v}\frac{du_{3,v}}{dt} + \dot{m}_{23,v}u_{3,v} = \dot{Q}_{3,e} + \dot{m}_{23,v}h_{2,v} - \dot{Q}_{3,w} \quad (6)$$

where $\dot{Q}_{3,e}$ represent the heat flow and the work exchanged per unit of time towards the outdoor environment respectively, $\dot{m}_{23,v}h_{2,v}$ represents the heat flow supplied by the steam accumulator during the tank filling and $\dot{Q}_{3,w}$ is the heat flow from the steam to the food product. The derivative of $u_{3,v}$ can be expressed as

$$\frac{du_{3,v}}{dt} = c_v dT_{3,v} + \left[T_{3,v} \left(\frac{\partial p_3}{\partial T_{3,v}} \right)_v - p_3 \right] dv_{3,v} \quad (7)$$

Using the Redlich-Kwong EoS to define the pressure p_3 [41], and computing the partial derivative of the pressure with respect to the temperature at constant volume, Eq. (7) can be integrated between a generic time instant t and the initial reference one t_0, obtaining

$$u_{3,v}(t) = u_{3,v}(t_0) + c_v\left(T_{3,v}(t) - T_{3,v}(t_0)\right) + \frac{3a}{2b\sqrt{T_{3,v}(t)}} \left[\log\left(\frac{V_{3,v} + b\, m_{3,v}(t_0)}{V_{3,v} + b\, m_{3,v}(t)} \right) \right] \quad (8)$$

where a and b represent two parameters of the Redlich-Kwong Eos [41] depending on the type of fluid. Substituting Eqs. (7) and (8) into Eq. (6), the state equation of the steam temperature $T_{3,v}$ can be expressed

$$\frac{dT_{3,v}}{dt} = \frac{\dot{m}_{23,v}}{C_I} \left(h_{2,v} - C_{II} + \frac{3\, a\, m_{3,v}}{2\left(V_{3,v} + b\, m_{3,v}\right)\sqrt{T_{3,v}}} \right) - \frac{\left(\dot{Q}_{3,w} - \dot{Q}_{3,e}\right)}{C_I} \quad (9)$$

with

$$C_I = m_{3,v} c_v - \frac{3 a m_{3,v}}{4 b T_{3,v}^{1.5}} \left[\log\left(\frac{V_{3,v} + b m(t_0)_{3,v}}{V_{3,v} + b m_{3,v}} \right) \right]$$

end

$$C_{II} = u(t_0)_{3,v} + c_v\left(T_{3,v} - T(t_0)_{3,v}\right) + \frac{3a}{2bT_{3,v}^{0.5}} \left[\log\left(\frac{V_{3,v} + bm(t_0)_{3,v}}{V_{3,v} + bm_{3,v}} \right) \right].$$

The state equation of the steam pressure p_3 can be obtained by deriving the Redlich-Kwong EoS [41] as

$$\frac{dp_3}{dt} = C_{III} \frac{dT_{3,v}}{dt} + C_{IV} \frac{V_{3,v}}{m_{3,v}^2} \dot{m}_{23,v} \quad (10)$$

with

$$C_{III} = \frac{R}{v_{3,v} - b} + \frac{a}{2\left(v_{3,v}^2 + b v_{3,v}\right) T_{3,v}^{1.5}}$$

and

$$C_{IV} = \frac{R\, T_{3,v}}{\left(v_{3,v} - b\right)^2} - \frac{a\left(2v_{3,v} + b\right)}{\left(v_{3,v}^2 + b v_{3,v}\right)^2 \sqrt{T_{3,v}}} .$$

The set of Eqs. (9) and (10) describes, thus, the steam temperature $T_{3,v}$ and pressure p_3 evolution in the processing tank during the filling phase.

3.3.2 Steam-food heat exchange model

Part of the steam flow rate injected in the processing tank condenses on the external surface of the food product. With the condensation process, a high quantity of energy is released by the steam with the formation of a thin film of water on the food surface, allowing a fast increment of the external temperature of the food product. The heat transfer coefficient $h_{3,w}$ between steam and food product was estimated by using the Nusselt correlation [42-43] and, in particular, the heat flow $\dot{Q}_{3,w}$ can be written as

$$\dot{Q}_{3,w} = \bar{h}_{3,w} A_{3,f} \left(T_{3,sat} - T_{3,f}\right) = \dot{m}_{3,c} \bar{\Lambda}_{3,w} \quad (11)$$

where $\bar{h}_{3,w}$ is the corrected form of the heat transfer coefficient $h_{3,w}$ during condensation [44-46], $A_{3,f}$ is the heat exchange surface between steam and food product, $T_{3,sat}$ and $T_{3,f}$ are the steam saturation temperature at pressure p_3 and the food product temperature respectively, $\dot{m}_{3,c}$ the mass rate of steam condensation on the product and $\bar{\Lambda}_{3,w}$ the corrected latent heat during condensation. The condensed water, once collected in the lower part of the processing tank and separated by a grid from the food to be processed, is discharged at the batch cycle completion.

The corrected heat transfer coefficient $\overline{h}_{3,w}$ takes into account three aspects: (a) the presence of superheated steam and subcooled condensate, (b) the presence of air and (c) the arrangement layout of the food product inside the processing tank.
More in detail:
The presence of superheated steam during the pressurisation and subcooled condensate, due to the food product temperature lower than the condensation temperature of the steam at pressure p_3, leads to an increment of the heat transfer coefficient [47]. To consider the sensible amount of energy transmitted between the steam and the food product, the corrected latent heat $\overline{\Lambda}_{3,w}$ is

$$\overline{\Lambda}_{3,w} = c_{p,shs}\left(T_{3,shs} - T_{3,sat}\right) + \Lambda_{3,w} + \frac{3}{8}c_{p,w}\left(T_{3,sat} - T_{3,f}\right) \quad (12)$$

where $c_{p,shs}$ is the specific heat of the superheated steam at constant pressure, $T_{3,shs}$ is the superheated temperature of the steam equal to $T_{3,v}$ when $T_{3,v} > T_{3,sat}$, $c_{p,w}$ is the water film specific heat.
The reduction of the heat transfer coefficient $h_{3,w}$ due to the presence of air, which does not condensate, can be taken into account accordingly to [48-49] by introducing the F_a coefficient

$$F_a = 0.5 \cdot \left[e^{\left(-47.7294\, y_a^{0.6246}\right)} + e^{\left(-2.8235\, y_a^{0.3533}\right)}\right] \quad (13)$$

where y_a is the ratio between the air mass and the total mass (air and steam).
The food product arrangement into the processing tank, reducing the overall food surface involved in the heat exchange due to overlapping layers, can be taken into account with the corrective coefficient $n^{-0.25}$ [50-51].
Based on the proposed considerations, the corrected heat transfer coefficient results

$$\overline{h}_{3,w} = F_a \frac{\alpha}{n^{0.25}}\left[\frac{\rho_{3,w}\left(\rho_{3,w} - \rho_{3,sat}\right) g\, \overline{\Lambda}_{3,w}\, k_{3,w}}{\mu_{3,w}\left(T_{3,w} - T_{3,f}\right) L_{3,f}}\right]^{0.25}. \quad (14)$$

where $\rho_{3,w}$ and $\rho_{3,sat}$ are the densities of the water film and of the steam at saturation pressure p_3 respectively, $k_{3,w}$ and $\mu_{3,w}$ are the thermal conductivity and viscosity of the water film, g is the gravitational acceleration, $L_{3,f}$ is the characteristic length of the food product defined as the ratio between the volume and the external surface, and α is a coefficient that depends on the geometry of the food product. The thermal properties $\rho_{3,w}$, $k_{3,w}$ and $\mu_{3,w}$ have to be calculated taking into account the water film temperature $T_{3,w}$, expressed as the mean temperature between the steam saturation temperature and the temperature of the food product.

3.3.3 Processing tank complete system of differential equations

By using $\overline{h}_{3,w}$, $A_{3,f}$, $T_{3,sat}$, $T_{3,f}$ and $\overline{\Lambda}_{3,w}$, it is possible to calculate the heat transfer rate $\dot{Q}_{3,w}$ in Eq. (11) and the steam condensation rate $\dot{m}_{3,c}$. Besides the state variables $T_{3,v}$ and p_3 (Eqs. (9) and (10)), vapour mass $m_{3,v}$, condensed liquid mass $m_{3,l}$ and mean temperature of the food product $T_{3,f}$ have to be studied.
The vapour mass $m_{3,v}$ and condensed liquid mass $m_{3,l}$ can be obtained by integrating over the time the steam flow rate $\dot{m}_{23,v}$ and steam condensation rate $\dot{m}_{3,c}$.
Hence, the dynamics of the processing tank state is described by the system of differential equations (SoDE)

$$\begin{cases} \dfrac{dT_{3,v}}{dt} = \dfrac{\dot{m}_{23,v}}{C_I}\left(h_{2,v} - C_{II} + \dfrac{3am_{3,v}}{2\left(V_{3,v} + bm_{3,v}\right)\sqrt{T_{3,v}}}\right) - \dfrac{\left(\dot{Q}_{3,w} - \dot{Q}_{3,e}\right)}{C_I} \\ \dfrac{dp_3}{dt} = C_{III}\dfrac{dT_{3,v}}{dt} + C_{IV}\dfrac{V_{3,v}}{m_{3,v}^2}\dot{m}_{23,v} \\ \dfrac{dm_{3,v}}{dt} = \dot{m}_{23,v} - \dot{m}_{3,c} \\ \dfrac{dm_{3,l}}{dt} = \dot{m}_{3,c} \\ \dfrac{dT_{3,f}}{dt} = \dfrac{\dot{Q}_{3,w}}{m_{3,f}c_{p,f}} \end{cases} \quad (15)$$

where the temperature of the food product $T_{3,f}$ is obtained by using a lumped parameter model with the food product mass $m_{3,f}$ and specific heat $c_{p,f}$.

3.4 Accumulator-to-processing tank steam flow rate model

The processing tank is connected to the steam accumulator by a pipe of constant section S_p with an on-off valve ψ_2 that can intercept the steam flow rate $\dot{m}_{23,v}$ (Fig. 1). When the valve ψ_2 is open, $\dot{m}_{23,v}$ is not constant, since the pressure of the upstream and downstream interconnected tanks varies over time. A similar problem can be found in the case of gas vehicle reservoirs fuelling [52-55].

In order to evaluate the evolution of $\dot{m}_{23,v}$, the steam velocity w_v can be derived applying the energy conservation of steam between the steam accumulator (section 2 in Fig. 1) and the pipe connection (section P in Fig. 1), by using the differential form of the first principle of thermodynamics

$$dq_v = dl_m + d(p_v v_v) + d\left(u_v + \frac{w_v^2}{2} + gz\right) \quad (16)$$

Neglecting the terms dq_v, dl_m and dgz (no significant potential energy variation), and by using the definition of enthalpy, the steam velocity value $w_{p,v}$ in the connection pipe can be computed as

$$w_{p,v} = \sqrt{2\left(h_{2,v} - h_{p,v}\right)} \quad (17)$$

where $h_{2,v}$ and $h_{p,v}$ are the steam enthalpy inside the steam accumulator and in the connection pipe. Considering section 2 not close to the inlet of the connection pipe, as reported in Fig. 1, steam velocity in the steam accumulator can be neglected.

Using the corrected ideal gas EoS [56]

$$pv = ZRT \quad (18)$$

the enthalpy can be written as

$$h_v = c_v T_v + ZRT_v = \frac{1}{(\gamma - 1)}\left(\gamma + \frac{1 - Z}{Z}\right)p_v v_v \quad (19)$$

where γ is the adiabatic coefficient of expansion. The value of the compressibility factor Z, equal to 0.93, was settled considering saturated steam at 8 bar pressure [56]. Substituting Eq. (19) in Eq. (17), the steam velocity can now be written as a function of the pressure and of the specific volume of steam in the accumulator and in the connection pipe as

$$w_{p,v} = \sqrt{\frac{2}{(\gamma - 1)}\left(\gamma + \frac{1 - Z}{Z}\right)\left(p_2 v_{2,v} - p_p v_{p,v}\right)} \; ; \quad (20)$$

where the specific volume and the pressure can be related considering the expansion of the steam from the accumulator to pipe being adiabatic.

By using Eq. (20) and considering an uniform flow in the connection pipe of constant section S_p, the steam flow rate $\dot{m}_{23,v}$ can be written as

$$\dot{m}_{23,v} = S_p \sqrt{C_V p_p \rho_{2,v} \left[\left(\frac{p_p}{p_2}\right)^{2/\bar{\gamma}} - \left(\frac{p_p}{p_2}\right)^{\bar{\gamma}+1/\bar{\gamma}} \right]} \quad (21)$$

where $\bar{\gamma}$ is the corrected adiabatic coefficient ($\bar{\gamma} = (\gamma - 1)Z + 1$) and the term C_V is equal to $C_V = \frac{2}{\gamma - 1}\left(\gamma + \frac{1 - Z}{Z}\right)$.

When the ratio between p_p and p_2 is lower than the critical pressure ratio β_{cr}, expressed as

$$\beta_{cr} = \frac{p_p}{p_2} = \left(\frac{2}{\bar{\gamma} + 1}\right)^{\frac{\bar{\gamma}}{\bar{\gamma}-1}} \quad (22)$$

the steam flow rate $\dot{m}_{23,v}$ is critical otherwise it is in subcritical condition.

In the case of pressure ratio p_p/p_2 lower than β_{cr}, substituting Eq. (22) into Eq. (21), the critical steam flow rate $\dot{m}_{23,v}$ can be written as function of the sole pressure p_2 as

$$\left(\frac{\dot{m}_{23,v}}{S_p}\right)_{cr} = \sqrt{\frac{C_V C_{VI}}{2}(\bar{\gamma} - 1)\, p_2\, \rho_{2,v}} \quad (23)$$

where C_{VI} is equal to

$$C_{VI} = \left(\frac{2}{\bar{\gamma} + 1}\right)^{\frac{\bar{\gamma}+1}{\bar{\gamma}-1}}.$$

Thus, the steam flow rate $\dot{m}_{23,v}$ can be defined as

$$\dot{m}_{23,v} = \begin{cases} S_p \cdot \sqrt{C_V\, p_2\, \rho_{2,v} \left[\left(\frac{p_p}{p_2}\right)^{2/\bar{\gamma}} - \left(\frac{p_p}{p_2}\right)^{\bar{\gamma}+1/\bar{\gamma}} \right]} & \text{if} \quad \frac{p_p}{p_2} \geq \beta_{cr} \\ S_p \cdot \sqrt{\frac{C_V C_{VI}}{2}(\bar{\gamma} - 1)\; p_2\, \rho_{2,v}} & \text{if} \quad \frac{p_p}{p_2} < \beta_{cr} \end{cases}. \quad (24)$$

Computing the pressure losses in the pipe Δp_p, the pressure p_p at the pipe inlet can be derived by the pressure in the processing tank p_3, as

$$p_p = p_3 + \Delta p_p(t) = p_3 + \frac{1}{2} f \frac{L_p}{D_p} \frac{\dot{m}_{23,v}^2}{\rho_{2,v}\, S_p^2} \quad (25)$$

where L_p and D_p are the pipe length and diameter of the pipe, f is the friction coefficient, calculated by using the Petukhov relation [56].

3.5 Model implementation

The presented model has been implemented in Matlab® environment (2015b version). The final number of differential equations (DE), fully describing the dynamics of the considered plant system, results to be seven, organized as follow: 2 DE for the steam accumulator state variables (Eqs. (2-3)), 5 DE for the processing tank (Eq. (15)). A scheme of the relationship between the model variables is represented in Fig. 2. The developed modelling framework allows to obtain the temporal variation of the thermodynamic state of the steam accumulator and of the processing tank, to evaluate the steam flow rate between the steam accumulator and the processing tank as a function of pressure difference of the tanks and also to calculate the food mean temperature during the thermal process. The initial conditions of the modelled system at time t_0 are reported on top of the scheme, while the set of plant parameters, such as the volume of the

steam accumulator, the connection pipe section, the food product heat exchange surface etc. have been omitted in the scheme.
The developed modelling framework can be profitably used during the designing phase of steam accumulators. Indeed, the parameterised model and initial plant conditions take into account all the typical sizing parameters and operative condition of these type of plants, allowing to find the proper configuration of boiler/steam accumulator/processing tank system.

3.5.1 Validation of the steam accumulator model

The results obtained by the proposed model were compared to data provided by [21] and [23], adopting the same parameters and initial conditions. Three validation tests were performed, where the accumulator charging and discharging processes have been simulated considering the three different steam flow rates reported in Fig. 3, from time instant $t_0 = 0$ and $t_f = 700$ seconds. The complete set of parameters and initial conditions, such as steam accumulator volume and pressure, inlet steam flow rate, etc., is collected in Table 1. More in detail, tests A and C were conducted considering the constant steam flow rate $\dot{m}_{12,v}$ and $\dot{m}_{23,v}$ respectively [21], while the test B has been performed with a time-varying steam flow rate $\dot{m}_{12,v}$ [23]. Mass flow rate, pressure and temperature as a function of time have been shown in Fig.3 for three different conditions.
The simulation results, reported in Fig. 4, have been compared with the ones presented in [21] and [23], which have been reported in the same plot. The final steady state conditions and the times required to reach them are comparable. In addition, the accordance between the charging and discharging dynamics provided by the model and by the references has been quantified calculating $\ell_\infty$and ℓ_2 norms based relative distances ε_∞ and ε_2 (Table 2) between the two functions $p_2(t)$ and $\hat{p}_2(t)$, the simulated time evolution of accumulator pressure and the reference one respectively. On the base of the obtained values for ε_∞ and ε_2, the developed steam accumulator model, based on the equilibrium conditions between vapour and liquid phases, can be considered adequately accurate to simulate different operating conditions.
In [21] and [23], authors demonstrate how the approximations introduced by considering an equilibrium model translates in an estimation error in the prediction of the real maximum and minimum pressure values, with respect to the non-equilibrium model. However, the maximum detected differences between the non-equilibrium and the equilibrium model, for some operating conditions, result to be around 6%, and occur at valves opening/closure [23]. Moreover, the non-equilibrium model requires the measurement of a set of parameters on a physical existing plant, preventing its adoption in the sizing stage.

4. A case study: debacterisation of cocoa beans

The developed modelling framework was applied to the debacterisation process of cocoa beans, a typical batch thermal process in the food industry. The debacterisation process is preceded by a cleaning phase to remove waste materials and a roasting phase to intensify the aroma of the cocoa beans. In order to satisfy the quality and safety regulatory standards in food production, once the roasting process is completed, the bacterial charge of the cocoa beans has to be further reduced by a steam treatment. Therefore, the roasted cocoa beans, still at a temperature of about 90-100 °C, are collected into a debacterisation tank. Once filled with the product and sealed, the processing tank is heated by steam insufflation, adopted to provide the heat for the debacterisation process.
Since a portion of the steam into the vessel, when it comes into contact with the cocoa beans surface, condenses forming a thin film of hot water, particular technical solutions must be introduced in order to

limit the condensed water to the quantity that does not compromise the food product. This can be achieved reducing as much as possible the time interval between the roasting and the debacterisation phases, in order to maintain a high beans surface temperature.
To further reduce condensation phenomena in the processing tank, it can be encased and pre-heated, so that the processing tank surface in contact with the food product is maintained at high temperature. In this case study, the considered processing tank layout allowed to assume thermal losses to the environment to be negligible.
After a fast pressurisation of the tank, which has a duration of 3 to 5 seconds, cocoa beans are mechanically mixed in order to assure the required uniformity to the debacterisation process. Usually, the mixing of cocoa beans is maintained throughout the entire duration of the process, which lasts about 5/10 minutes and finishes with the cocoa beans unloading procedure. Since the objective of this study is to model the pressurisation of the processing tank by the concurrent depressurisation of the steam accumulator, the mixing process of cocoa beans has not been considered in this model.

4.1 Simulation setup

At initial time t_0, the steam accumulator has been considered at a pressure $p_2(t_0)$ slightly lower than the maximum settled value $p_{2,max}$, while the debacterisation tank is, initially, in equilibrium with the environment pressure. The temperature of the cocoa beans to be processed, when placed in the debacterisation tank, has been considered equal to 95 °C when the thermal treatment starts, after the valve ψ_2 opening. All the geometrical and physical properties of the plant components, together with their standard initial working conditions, are summarised in Table 3 organised by four groups: (1) the steam boiler; (2) the steam accumulator; (3) the debacterisation tank and (4) the connection pipe between the tanks [57].
In order to evaluate the heat exchange area $A_{3,f}$ between the water film and the food product, the shape of the cocoa beans was approximated to a geometrical shape made by a parallelepiped, the base of which has dimensions, a_{cb} and b_{cb} and a lateral area is considered rounded with a radius of $d_{cb}/2$, half of the parallelepiped height (Fig. 5). The dimensions a_{cb}, b_{cb} and d_{cb} have been considered equal to 2 cm, 1 cm and 0.4 cm respectively. Since in the debacterisation tank the cocoa beans are arranged in multiple layer, resulting in a vertical sequence of overlapping items, only the curved surface has been taken into account as heat exchange area between the water film and the cocoa beans. The resulting value of $A_{3,f}$ is used in Eq. (11) to evaluate $\dot{Q}_f$, while the coefficient α of Eq. (14), in the case of the cocoa beans geometry, is equal to 0.815. Moreover, the influence on the pressurisation process of the set of plant initial and working conditions, constituted by the accumulator maximum pressure $p_{2,max}$ and the filling ratio $\xi_{2,l}$, has been investigated. The effect of the plant components size (accumulator volume V_2 and connection pipe diameter D_p) in the process has been also analysed by simulations conducted with the developed modelling framework. All the simulations have been performed varying one parameter at time, while maintaining all the others settled to the values adopted during the initialization of the first case study (Table 3).

4.2 Simulation results

The model provides the time evolution of the thermodynamic state of the steam accumulator and of the debacterisation tank, the time evolution of the steam flow rate between the two tanks and the temperature evolution of the cocoa beans. Since the simulations confirmed the rapidity of the pressurisation process of the debacterisation tank, which mainly occurs in the first two seconds after the valve ψ_2 opening, the graphical output focuses on a short period of time, ten seconds long. During the first

part of the simulation, the accumulator is charged by the steam flow $\dot{m}_{12,v}$, since $t_0 = 0$ s until $t_1 = 4.3$ s. At t_1, time instant when the accumulator pressure reaches the maximum settled value $p_{2,max}$, the valve ψ_1 is closed (Fig. 6). During this phase, valve ψ_2 is still closed.

The pressurisation of the debacterisation tank starts at time instant $t_2 = 5$ s, when valve ψ_2 is opened and the steam flow rate $\dot{m}_{23,v}$ is established. During the pressurisation, a rapid increment of the pressure p_3 in the debacterisation tank and a concurrent decrease of the pressure p_2 occur (Fig. 7), until an equilibrium between the pressure in the steam accumulator and the pressure in the processing tank is reached. It can be noted that, the equilibrium condition is reached in about two seconds, approximately at time instant $t_3 = 7$ s, when the pressure p_3 in the debacterisation tank reaches the maximum value, of about 7.75 bar. The steam flow rate $\dot{m}_{23,v}$ between the two tanks is critical, reaching its maximum value of 2.11 kg s^{-1}, in the initial part of the pressurisation (time interval $t \in [5;\ 5.5]$ s), becoming sub-critical in the remaining part of the pressurisation (Fig. 6). It can be noted that, at the end of this process, the pressure $p_2(t_2)$ of the accumulator is slightly lower than the initial value $p_2(t_1)$, which was about 8 bar (Fig. 7). This behaviour can be caused by two main conditions: (1) the debacterisation tank volume V_3 is 4 times smaller than the steam accumulator one, V_2; (2) the pressurisation of the debacterisation tank is fast, therefore the steam mass exiting the steam accumulator, required to pressurised the processing tank, is small compared to the overall steam mass available in the accumulator. Even if the maintenance of a high pressure value p_2 during the accumulator discharge is a valuable property, the simulation shows an oversizing of the installed accumulator, considering the sole debacterisation user process.

After the time instant t_3, when the pressurisation process of the debacterisation tank can be considered completed (the pressure p_3 becomes stationary, settled at the maximum value), a secondary phenomenon can be noticed. The accumulator discharge does not end after the pressurisation of the debacterisation tank: the steam flow rate $\dot{m}_{23,v}(t)$, with $t \in [7;\ 10]$ s, is settled to a low value, about 0.08 kg s^{-1}, without becoming completely null, and a remarkable change of the curve slope of the pressure p_2 denotes a slower dynamic in the system. This can be addressed to the slow condensing process of part of the steam $m_{3,v}$ in the debacterisation tank, which leads to a gradual decrement of the pressure p_3 and, thus, to the consequent re-balancing steam flow $\dot{m}_{23,v}$.

A contribution to the fast dynamic of the steam temperature $T_{3,v}$ in the debacterisation tank (Fig. 8) is caused by the pressure work of the steam flow rate $\dot{m}_{23,v}$, which contributes to the debacterisation tank internal energy increment. During the initial phase of the debacterisation process, the physical phenomenon of the pressurisation of the tank prevails over the heat exchange from the steam to the cocoa beans. After t_2, the steam flow rate $\dot{m}_{23,v}$ decrement leads to a reduction of the heat provided to the processing tank from the accumulator, which becomes lesser than the one transferred to the cocoa beans: the steam temperature $T_{3,v}$ in the debacterisation tank, thus, starts decreasing. At the end of the simulation, the steam mass $m_{3,v}$ in the debacterisation tank is about 3 kg while the final mass of condensed steam $m_{3,l}$ on the cocoa beans surfaces results to be limited at about 0.2 kg, fulfilling the need of avoiding food product damages.

Further simulations have been carried out to investigate the effects of some operating conditions (e.g. maximum pressure of the steam accumulator) and of the sizing parameters (e.g. volume of the steam accumulator) on the dynamic evolution of the steam in the interconnected tanks. The most significant results of the simulations are reported in Figs. (9-14).

Varying the maximum pressure of the accumulator, with values ranging from 8 to 6 bar, the evolution of the pressure in the steam accumulator and in the processing tank results to be modified as reported in Fig. 9. During the pressurisation of the processing tank, the pressure of the accumulator slightly decreases,

reaching the steady state pressure values in around 2 seconds: 6.80 and 5.83 bar with $p_{2,max}$ settled to 7 and 6 bar respectively. The effect on the steam flow rate $\dot{m}_{23,v}$ of the pressure difference between the accumulator and the processing tank can be observed in Fig. 10 where, after the valve ψ_2 opening ($t_2 = 5$ s), the maximum value of the steam flow value decreases from 2.11 kg s^{-1} to 1.60 kg s^{-1} with the $p_{2,max}$ decrement.

Acting on the filling ratio of the steam accumulator, a variation in the charging and discharging dynamic of the steam accumulator can be achieved. In particular, comparing the simulation results obtained with $\xi_{2,l}$ equal to 0.4 and 0.6 with those obtained with $\xi_{2,l} = 0.5$, a reduction of the charging process duration is observed in the case of filling ratio decrement (Fig. 11). Indeed, the mass of liquid to be heated up, in this case, is less and the energy required for the accumulator pressurisation is, thus, lower. Similarly, during the accumulator discharging process, a faster decrement of the pressure can be observed, because of the lower quantity of water (or energy) stored in the accumulator.

Steam plant sizing parameters have been also analysed. In particular, by considering steam accumulators with smaller volumes, during the charging process the maximum pressure $p_{2,max}$ of 8 bar can be achieved in shorter times (Fig. 12). This behaviour is due to the small quantity of water to be heated up, which also affect the discharging phase. Indeed, after ψ_2 opening at time t_2, the user steam request lead to a faster depressurisation and to lower final pressure steady state in the accumulators with reduced volume (Fig. 12). It can be observed that, at the end of the simulation $t_4 = 10$ s, the final pressure in steam accumulator accounts for 7.81 and 7.71 bar with a steam accumulator volume of 3 and 2 m^3 respectively.

The effect to the steam flow rate of the pipe connection between the accumulator and the processing tank has been also investigated. In particular, by varying the section of the pipe, in the conducted simulations the maximum steam flow rate reduces from 2.11 kg s^{-1} to 1.38 kg s^{-1} (Fig.13), considering pipe diameters values of 5, 4.5 and 4 cm. Even if the final steady state pressure in the two interconnected tanks results to be equal (Fig. 14), the pressure evolutions differ, being the time required to reach the equilibrium condition increased by the pipe diameter reduction.

5. Conclusions

In this paper, a model of a food processing plant, constituted by a boiler, a sliding pressure steam accumulator and a processing tank has been presented. The developed model, based on the mass and energy balances, also integrates the properties of the processed food in the last tank. The condensation and evaporation processes in the steam accumulator were approximated with a succession of equilibrium state and the steam flow rate from this vessel to the processing pressurised tank was evaluated as a function of the pressure difference between the two tanks. The model has been also applied to a real system configuration for cocoa beans debacterisation; nevertheless, with limited appropriate changes, it can be profitably adapted to a wide set of different thermal processes of food industry employing sliding pressure steam accumulators to feed pressurised tanks.

Allowing to simulate the dynamics of a complete set of plant state variables, such as pressures, temperatures and flow rate/masses, during processes with different settings and initial conditions, the developed modelling framework has already proven its effectiveness in designing new processing plants. The sizing of the steam accumulator as well as the operative settings, such as the boiler steam supply pressure and flow rate, the initial water filling ratio of the accumulator etc., can be evaluated in advance for a wide range of plant configurations, allowing, for example, to properly size a system composed of steam boiler and steam accumulator when the steam demand profile of a user is known.

Table 1. Accumulator parameters and initial conditions of validation tests

	Test A	Test B	Test C
volume V_2 of the steam accumulator [m^3]	64	64	64
water filling ratio $\xi_{2,l}$ of the steam accumulator	0.5	0.5	0.5
initial pressure p_2 of the steam accumulator [bar]	25	-	50
initial state of valve ψ_1	open	closed	open
initial state of valve ψ_2	closed	open	closed

Table 2. ℓ_∞ and ℓ_2 norms based relative distances between model and reference dynamics

	Test A	Test B	Test C
$\varepsilon_\infty = \frac{\lvert p_2(t^*) - \hat{p}_2(t^*)\rvert}{\lvert p_2(t^*)\rvert}$ with $t^* = \arg\max_{t\in[t_0,t_f]} \lvert p_2(t) - \hat{p}_2(t)\rvert$	0.0035	0.0114	0.0038
$\varepsilon_2 = \frac{\int_{t_0}^{t_f}\left(p_2(t) - \hat{p}_2(t)\right)^2 dt}{\int_{t_0}^{t_f}\left(p_2(t)\right)^2 dt}$	4.8013 10^{-6}	7.7657 10^{-5}	2.0237 10^{-6}

Table 3. Plant parameters and initial conditions of the case study simulation

Steam boiler	
nominal steam flow rate $\dot{m}_{12,v}$ [kg s^{-1}]	0.097
nominal pressure $p_{1,v}$ [bar]	8
Steam accumulator	
volume V_2 [m^3]	4
external surface A_2 [m^2]	14.5
thermal losses coefficient K_2 [W m^{-2} K^{-1}]	0.7
water filling ratio $\xi_{2,l}$	0.5
initial pressure p_2 [bar]	7.98
maximum pressure $p_{2,max}$ [bar]	8
Debacterisation tank	
volume V_3 [m^3]	1
initial pressure p_3 [bar]	1
initial temperature $T_{3,v}$ [°C]	100
initial temperature of cocoa beans $T_{3,f}$ [°C]	95
mass of cocoa beans $m_{3,f}$ [kg]	50
number of cocoa beans N	26,000
Connection pipe	
length of the pipe L_p [m]	5
diameter of the pipe D_p [m]	0.05

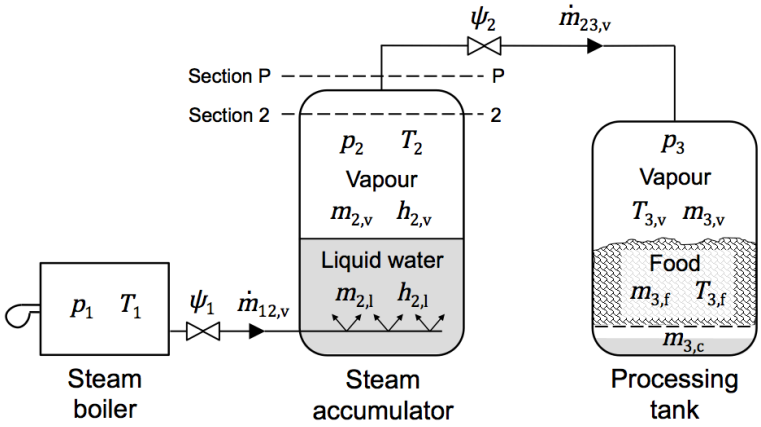

Figure 1. Scheme of a three-stage steam plant for batch thermal process of food products constituted by a steam boiler, a steam accumulator and a processing tank.

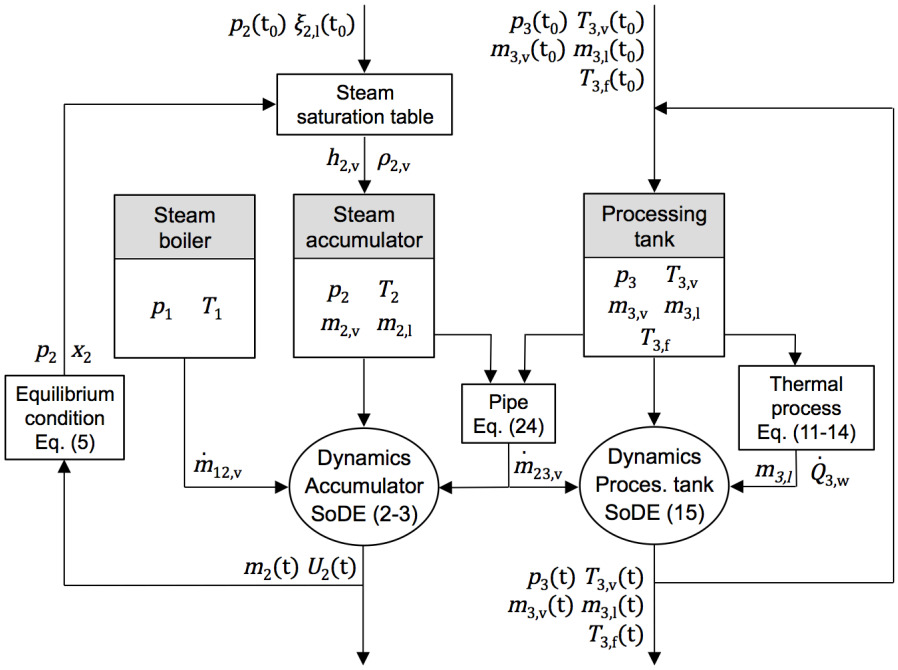

Figure 2. Illustrative scheme of the developed model.

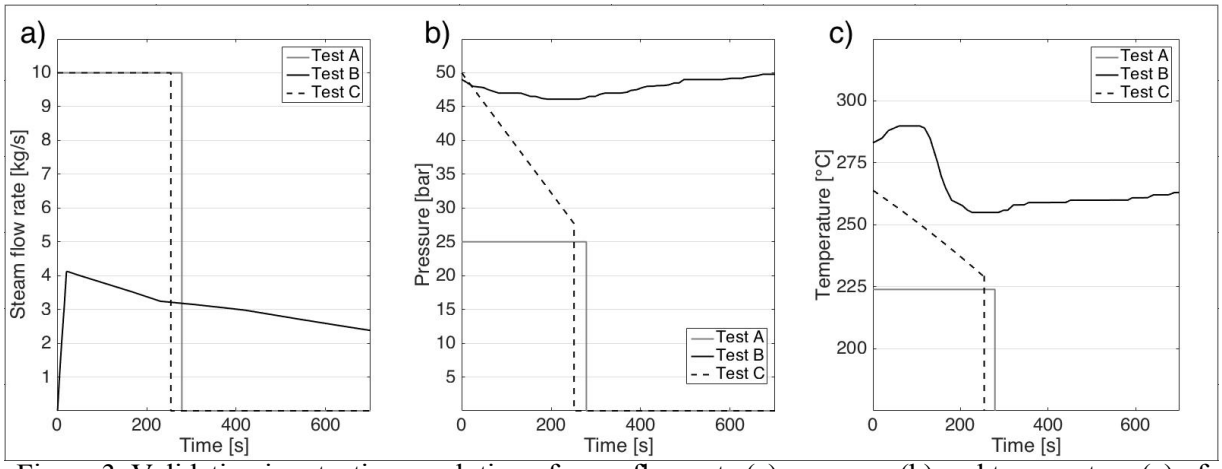

Figure 3. Validation inputs: time evolution of mass flow rate (a), pressure (b) and temperature (c) of the steam flows

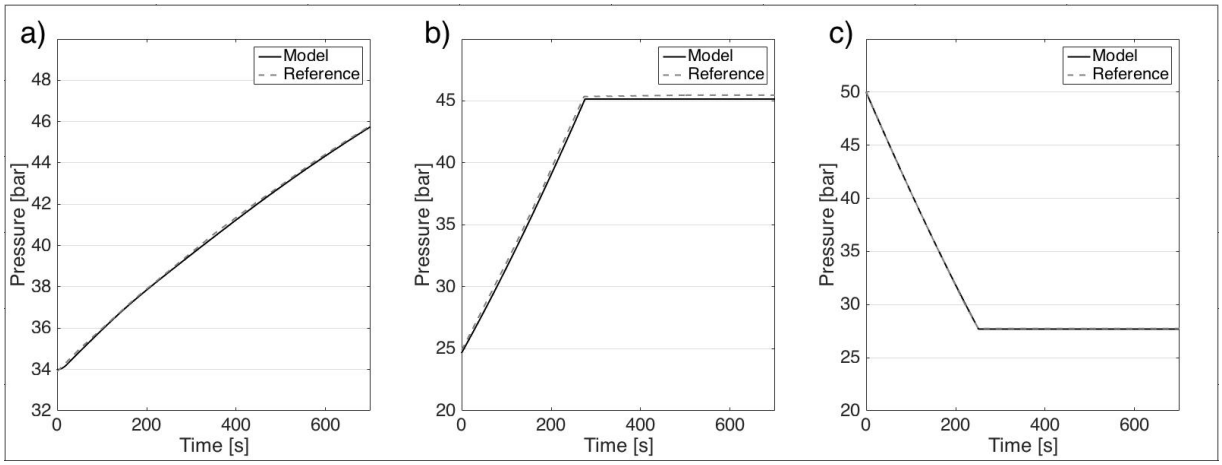

Figure 4. Validation results: time evolution of the pressure p_2 in the steam accumulator, resulting from the validation test A (a), test B (b) and test C (c).

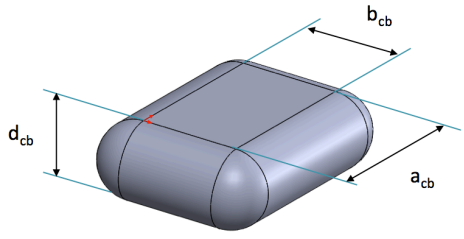

Figure 5. Modelling representation of cocoa bean

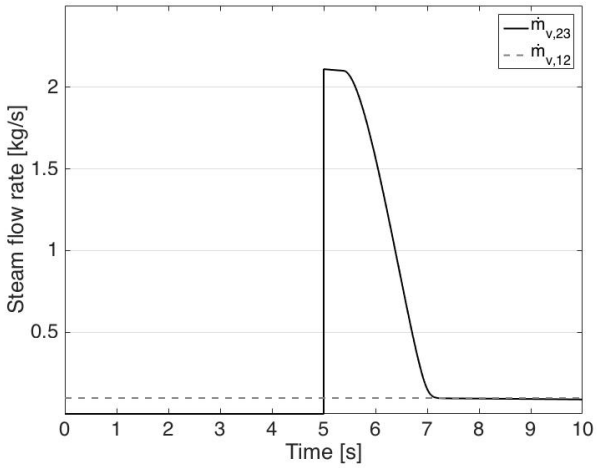

Figure 6. Time evolution of the steam flow rate $\dot{m}_{12,\mathrm{v}}$, from the steam boiler to the accumulator, and of the steam flow rate $\dot{m}_{23,\mathrm{v}}$, from the accumulator to the debacterisation tank.

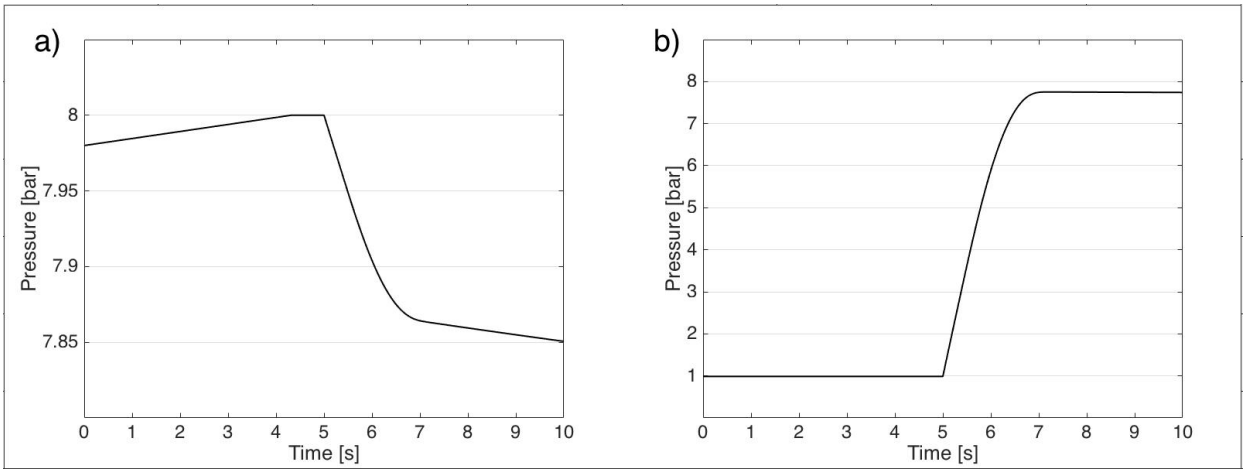

Figure 7. Time evolution of the pressures p_2 in the accumulator (a) and p_3 in the debacterisation tank (b)

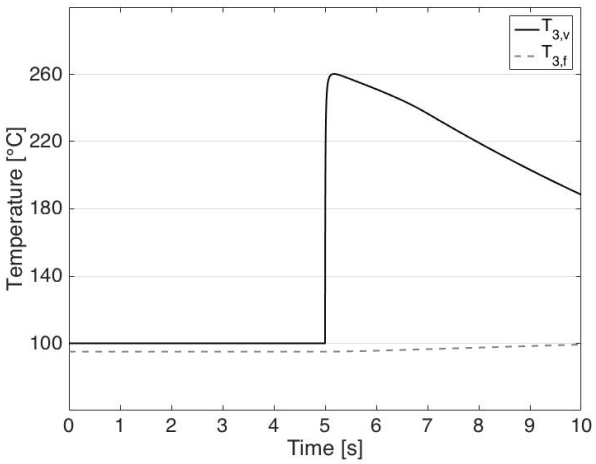

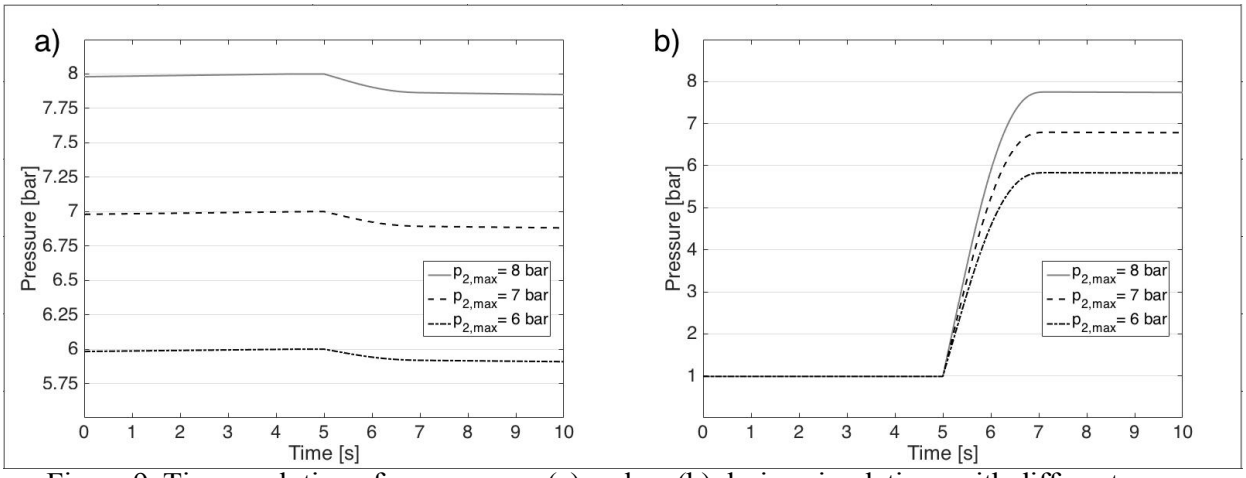

Figure 9. Time evolution of pressures p_2 (a) and p_3 (b) during simulations with different $p_{2,\max}$ values

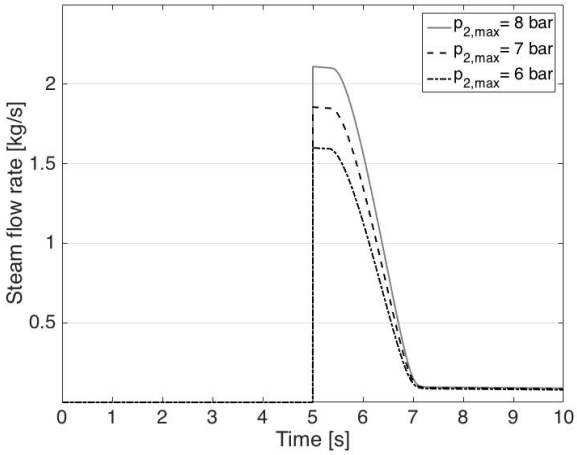

Figure 10. Time evolution of steam flow rate $\dot{m}_{23,\mathrm{v}}$ during simulations with different $p_{2,\max}$ values

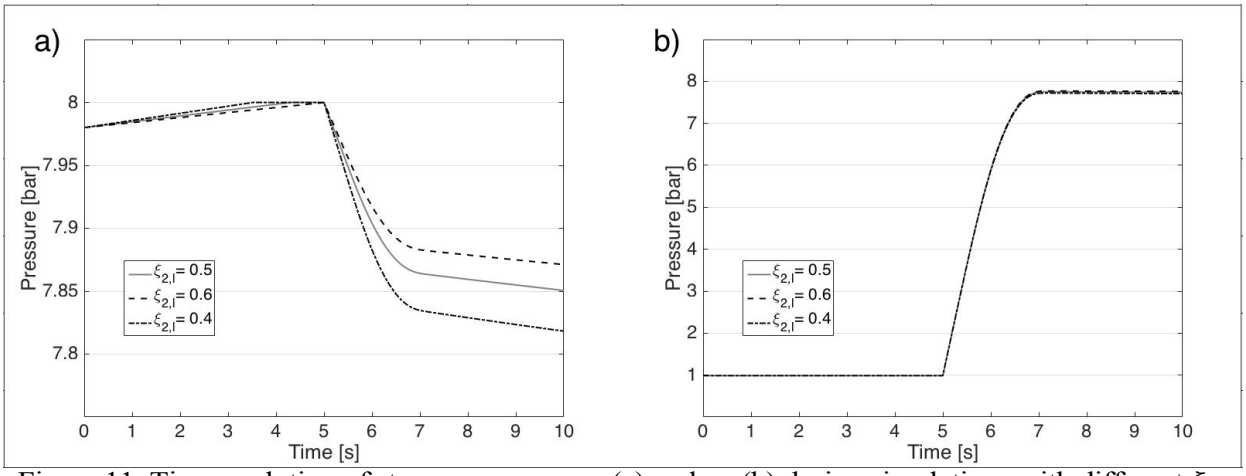

Figure 11. Time evolution of steam pressures p_2 (a) and p_3 (b) during simulations with different $\xi_{2,\mathrm{l}}$ values

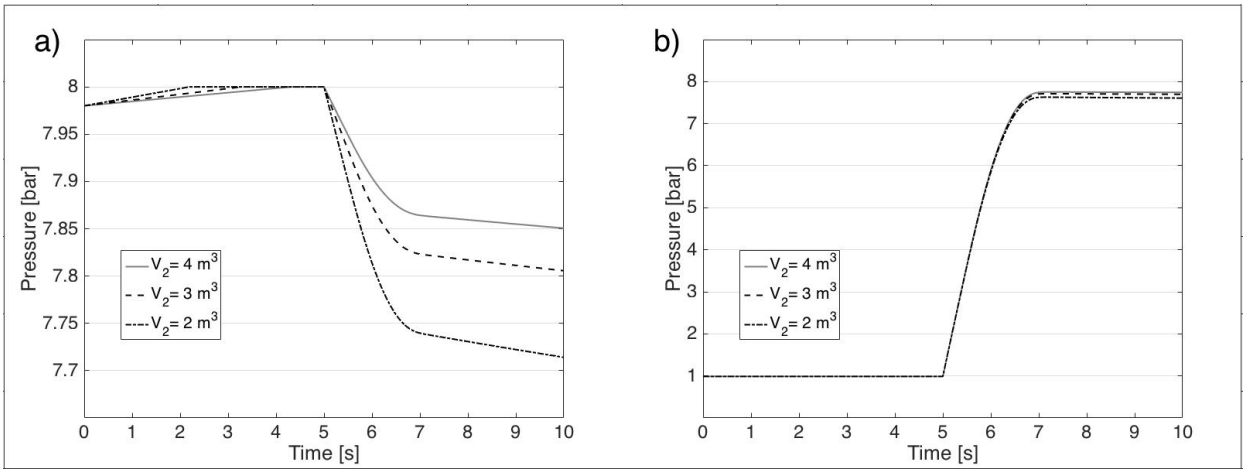

Figure 12. Time evolution of steam pressures p_2 (a) and p_3 (b) during simulations with different V_2 values

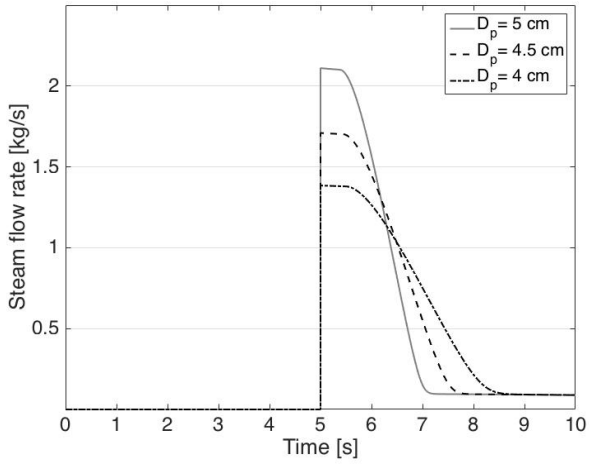

Figure 13. Time evolution of steam flow rate $\dot{m}_{23,\mathrm{v}}$ during simulations with different D_p values

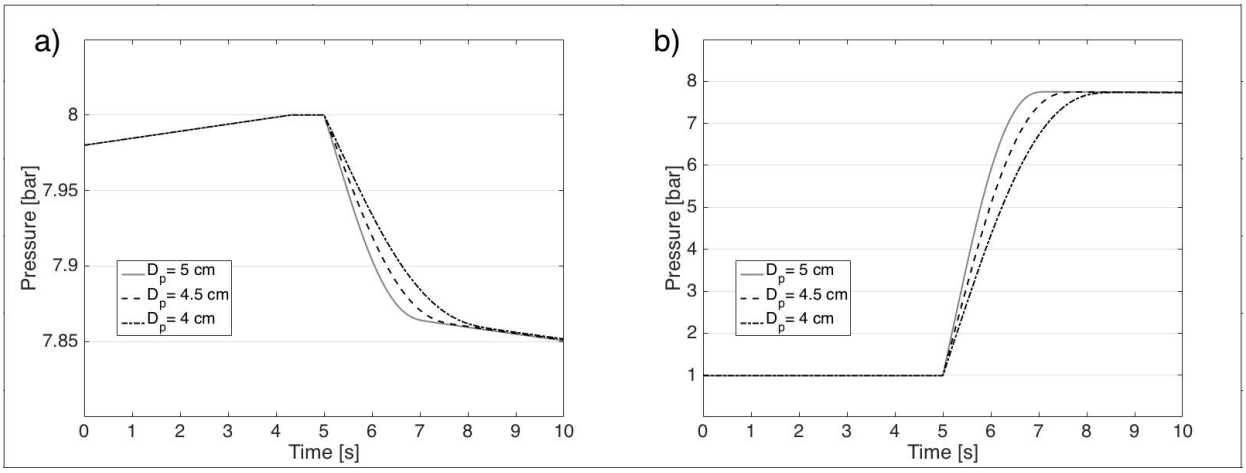

Figure 14. Time evolution of steam pressures p_2 (a) and p_3 (b) during simulations with different D_p values

Acknowledgements

Authors would like to thank Prof. Bruno Panella, Prof. Mario Malandrone and Guido Gobino S.r.l. for their support.

References

[1] M.E. Walker, Zhen Lv, E. Masanet. Industrial Steam Systems and the Energy-Water Nexus. Environ Sci Technol. 47 (2013) 13060-13067.

[2] Industrial Steam Systems Optimization (SSO) Experts Training. United Nations Industrial Development Organization, October 2012.

[3] K.W. Tam, C.W. Leung, S.D. Probert. Energy management in a dairy-products plant. Appl Energ. 32(2) (1989) 83-100.

[4] C. James, E.O. Göksoy, J.E.L. Corry, S.J. James. Surface pasteurisation of poultry meat using steam at atmospheric pressure. J Food Eng. 45 (2000) 111-117.

[5] T. Pirasaci, D. Yogi Goswami. Influence of design on performance of latent heat storage system for a direct steam generation power plant. Appl Energ. 162 (2016) 644-652.

[6] L. Sun, S. Doyle, R. Smith. Understanding steam costs for energy conversation projects. Appl Energ. 161 (2016) 647-655.

[7] B. Grange, C. Dalet, Q. Falcoz, A. Ferrière, G. Flamant. Impact of thermal energy storage integration on the performance of a hybrid solar gas-turbine power plant. Appl Therm Eng. 105 (2016) 266-275.

[8] G. Comodi, F. Carducci, B. Nagarajan, A. Romagnoli. Application of cold thermal energy storage (CTES) for building demand management in hot climates. Appl Therm Eng. 103 (2016) 1186-1195.

[9] H. Schreiber, S. Graf, F. Lanzerath, A. Bardow. Adsorption thermal energy storage for cogeneration in industrial batch processes: Experiment, dynamic modelling and system analysis. Appl Therm Eng. 89 (2015) 485-493.

[10] S.N. Palacio, K.F. Valentine, M. Wong, K.M. Zhang. Reducing power system costs with thermal energy storage. Appl Energ. 129 (2014) 228-237.

[11] D. Kishor Johar, D. Sharma, S. Lal Soni, P.K. Gupta, R. Goyal. Experimental investigation on latent heat thermal energy storage system for stationary C.I. engine exhaust. Appl Therm Eng. 104 (2016) 64-73.

[12] M. Cao, J. Cao. Optimal design of thermal-energy stores for boiler plants. Appl Energ. 83(1) (2006) 55-68.

[13] S. Cenkowski, C. Pronyk, D. Zmidzinska, W.E. Muir. Decontamination of food products with superheated steam. J Food Eng. 83 (2007) 68-75.

[14] F. Karimi. Applications of superheated steam for drying of food products. Int Agrophys. 24 (2010) 195-204.

[15] W. Zzaman, R. Bhat, T.A. Yang. Application of Response Surface Methodology to Optimize Roasting Conditions in Cocoa Beans Subjected to Superheated Steam treatments in Relevance to Antioxidant Compounds and Activities. Dry Technol. 32 (2014) 1104-1111.

[16] Steambook. Steam applications. Fischer.

[17] W.D. Steinmann, M. Eck. Buffer storage for direct steam generation. Sol Energy. 80 (10) (2006) 1277-1282.

[18] A. Baldini, G. Manfrida, D. Tempesti. Model of a solar collector/storage system for industrial thermal applications. Int J Thermodyn. 12 (2009) 83-88.

[19] E.S. Xu, Z.F. Wang, G. Wei. Dynamic simulation of thermal energy storage system of Badaling 1 MW solar power tower plant. Renew Energ. 39 (2012) 455-462.

[20] F. Bai, C. Xu. Performance analysis of a two-stage thermal energy storage system using concrete and steam accumulator. Appl Ther Eng. 31(14-15) (2011) 2764-2771.

[21] V.D. Stevanovic, B. Maslovaric, S. Prica. Dynamics of steam accumulation. Appl Therm Eng. 37 (2012) 73-79.

[22] B. Sun, J. Guo, Y. Lei, L. Yang, Y. Li, G. Zhang. Simulation and verification of a non-equilibrium thermodynamic model for a steam catapults steam accumulator. Int J Heat Mass Tran. 85 (2015) 88-97.

[23] V.D. Stevanovic, M.M. Petrovic, S. Milivojevic, B. Maslovaric. Prediction and Control of Steam Accumulation. Heat Transfer Eng. 36(5) (2015) 498-510.

[24] ASHRAE, ASHRAE Systems and Equipment Handbook. Atlanta (GA): ASHRAE; 2000.

[25] R.C.E. Ahlgren. Flash tanks for steam and boilers systems. ASHRAE J. 33(8) (1991) 15-20.

[26] M. Sakin-Yilmazer, T. Kemerli, H. Isleroglu, O. Ozdestan, G. Guven, A. Uren A et al. Baking kinectics of muffins in convection and steam assisted hybrid ovens. J Food Eng. 119 (2013) 483-489.

[27] L.J. Bowers, M.E. Dikeman, L. Murray, S.L. Stroda. Cooked yields, color, tenderness, and sensory traits of beef roasts cooked in an oven with steam generation versus a commercial convection oven to different endpoint temperatures. Meat Sci. 92 (2012) 97-106.

[28] B. Mora, E. Curti, E. Vittadini, D. Barbati. Effect of different air/steam convection cooking methods on turkey breast meat: Physical characterization, water status and sensory properties. Meat Sci. 88 (2011) 489-497.

[29] S.-R. Huang, J.I. Yang, Y.-C. Lee. Interactions of heat and mass transfer in steam reheating of starchy foods. J Food Eng. 114 (2013) 174-182.

[30] W.L. Lau, J. Reizes, V. Timchenko, S. Kara, B. Kornfeld. Numerical modeling of an industrial steam-air sterilization process with experimental validation. Appl Therm Eng. 75 (2015) 122-134.

[31] A.P. Singh, A. Singh, H.S. Ramaswamy. Modification of a static steam retort for evaluating heat transfer under reciprocation agitation thermal processing. J Food Eng. 153 (2015) 63-72.

[32] M.N. Berteli, A.A. Vitali, M.I. Berto, Jr A. Marsaioli. Alternative venting in steam retorts – An approach to energy savings in thermal processing. Chem Eng Process. 70 (2013) 204-210.

[33] M.J. Moran, H.N. Shapiro. Fundamentals of engineering thermodynamics. Fifth edition. Chichester: John Wiley & Sons; 2006.

[34] W. Wagner, H.J. Kretzschmar. International steam tables. Properties of water and steam based on the industrial formulation IAPWS-IF97. Second edition. Berlin: Springer: 2008.

[35] The First Law of Thermodynamics. In: C. Borgnakke, R.E. Sonntag. Fundamentals of Thermodynamics. 7th ed. John Wiley & Sons; 2009, p. 180-237.

[36] E. Ruffio, D. Saury, D. Petit. Thermodynamic analysis of hydrogen tank filling. Effects of heat losses and filling rate optimization. Int J Hydrogen Energ. 39 (2014) 12701-12714.

[37] M. Striednig, S. Brandstätter, M. Sartory, M. Klell. Thermodynamic real gas analysis of a tank filling process. Int J Hydrogen Energ. 39 (2014) 8495-8509.

[38] C. Li, Y. Peng, J. Dong. Prediction of compressibility factor for gas condensate under a wide range of pressure conditions based on a three-parameter cubic equation of state. J Nat Gas Sci Eng. 20 (2014) 380-395.

[39] Y.L. Liu, Y.Z. Zhao, L. Zhao, X. Li, H.G. Chen, L.F. Zhang, et al. Experimental studies on temperature rise within a hydrogen cylinder during refueling. Int J Hydrogen Energ. 35 (2010) 2627-2632.

[40] Q. Li, J. Zhou, Q. Chang, W. Xing. Effects of geometry and inconstant mass flow rate on temperatures within a pressurized hydrogen cylinder during refueling. Int J Hydrogen Energ. 37 (2012) 6043-6052.

[41] O. Redlich, J.N.S. Kwong. On The Thermodynamics of Solutions. Chem Rev. 44 (1949) 233-244.

[42] Condensation and Boiling Heat Transfer. In: J.P. Holman. Heat Transfer. 10th ed. New York: McGraw Hill; 2010, p. 487-520.

[43] Condensation. In: J.G. Collier, J.R. Thome. Convective Boiling and Condensation. 3rd ed. Oxford: Clarendon Press; 1994, p. 430-87.

[44] P. Sa-adchom, T. Swasdisevi, A. Nathakaranakule, S. Soponronnarit. Mathematical model of pork slice drying using superheated steam. J Food Eng. 104 (2011) 499-507.

[45] S. Soponronnarit, S. Prachayawarakorn, W. Rordprapat, A. Nathakaranakule, W. Tia. A Superheated-Steam Fluidized-Bed Dryer for Parboiled Rice: Testing of a Pilot-Scale and Mathematical Model Development. Dry Technol. 24 (2006) 1457-1467.

[46] S. Kittiworrawatt, S. Devahastin. Improvement of a mathematical model for low-pressure superheated steam drying of a biomaterial. Che Eng Sci. 64 (2009) 2644-2650.

[47] P.J. Marto. Condensation. In: W.M. Rohsenow, J.P. Harnett, Y.I. Cho, editors. Handbook of Heat Transfer. 3rd ed. McGrawhill; 1998, chap. 14.

[48] R. Rocca-Poliméni, D. Flick, J. Vasseur. A model of heat and mass transfer inside a pressure cooker. J Food Eng. 107 (2011) 393-404.

[49] W.L. Lau, J. Reizes, V. Timchenko, S. Kara, B. Kornfeld. Numerical modelling of an industrial steam-air sterilisation process with experimental validation. Appl Therm Eng. 75 (2015) 122-134.

[50] J. Rose, H. Uehara, S. Koyama, T. Fujii. Film Condensation. In: S.G. Kandlikar, M. Shoji, V.K. Dhir, editors. Handbook of Phase Change: Boiling and Condensation. Taylor & Francis; 1999, p. 523-80.

[51] Condensation. In: P.B. Whalley. Boiling, Condensation, and Gas-Liquid Flow. Oxford: Clarendon Press; 1987, p. 212-28.

[52] M. Farzaneh-Gord, S. Hashemi, A. Farzaneh-Kord. Thermodynamics Analysis of Cascade Reserviors Filling Process of Natural Gas Vehicle Cylinders. World Appl Sci J. 5 (2008) 143-149.

[53] M. Farzaneh-Gord, M. Deymi-Dashtebayaz. Optimizing natural gas fueling station reservoirs pressure based on ideal gas model. Pol J Che Technol. 15(1) (2013) 88-96.

[54] W.S. Winters, G.H. Evans, S.F. Rice, R. Greif. An experimental and theoretical study of heat and mass transfer during the venting of gas from pressure vessels. Int J Heat Mass Tran. 55 (2012) 8-18.

[55] K.J. Kountz. Modelling the fast fill process in natural gas vehicle storage cylinders. Institute of Gas Technology Chicago, IL 60632.

[56] Y.A. Çengel, M.A. Boles. Thermodynamics: An Engineering Approach. 5th ed. McGraw-Hill.

[57] A. Biglia, E. Fabrizio, M. Ferrara, P. Gay, D. Ricauda Aimonino. Performance assessment of a multi-energy system for a food industry. Energy Procedia 82 (2015) 540-545.